Clays and Clay Minerals, Vol. 47, No. 5, 647–657, 1999.

SELECTIVE GAS ADSORPTION BY AMORPHOUS CLAY-MINERAL DERIVATIVES

CRISTINA VOLZONE,[1] JOHN G. THOMPSON,[2] ALEXANDRA MELNITCHENKO,[2] JOSÉ ORTIGA,[1] AND STEPHEN R. PALETHORPE[2]

[1] Centro de Tecnología de Recursos Minerales y Cerámica (CETMIC), Consejo Nacional de Investigaciones Científicas y Técnicas (CONICET), Cno. Centenario y 506, CC 49 (1897) MB Gonnet, Buenos Aires, Argentina
[2] Research School of Chemistry, Australian National University, Canberra ACT 0200, Australia

Abstract—Amorphous derivates prepared by aqueous reaction of various aluminosilicate clay minerals with concentrated KF solution at 80–110°C were studied for their gas adsorption properties. The four clay minerals studied are halloysite, a well-crystallized kaolinite, a poorly crystallized kaolinite, and a montmorillonite. The gases tested are N_2, O_2, CH_4, CO, CO_2, and C_2H_2. The kaolin-group mineral derivatives are characterized by substantial reduction in particle size, high specific surface, and significant selectivity towards CO_2 and C_2H_2 relative to the other gases. The montmorillonite derivative shows no increase in adsorption over the starting material, however, for all the materials high adsorption of CO_2 and C_2H_2 was observed. Levels of gas adsorption and gas adsorption ratios are comparable to pillared clays.

Key Words—Amorphous Derivative, Gas Adsorption, Gas Separation, Halloysite, Kaolinite, Montmorillonite, Potassium Fluoride, CMS Source Clay SAz-1, Specific Surface.

INTRODUCTION

For the common clay minerals with no accessible internal surfaces, it is the external surface of the particles that determines their gas adsorption properties. By contrast, the gas adsorption properties of microporous solids, such as zeolites, pillared clays, sepiolite, and palygorskite, are dominated by the internal surface and sometimes the channel diameter. Among and within the clay mineral groups, there is a large variety of specific surfaces, corresponding to the wide range of particle sizes and shapes, ranging from <1 m^2g^{-1} for a coarse well-crystallized kaolinite or vermiculite to ~ 30 m^2g^{-1} for a very fine kaolinite to several hundred m^2g^{-1} for a partly delaminated montmorillonite.

Preferential adsorption of gases on sorbents can be used for gas separation purposes. The theory and practice of preferential adsorption for gas separation applications is treated by Yang (1987). Adsorptive separation can occur by three mechanisms. The first is due to steric effects such as the molecular-sieving property of zeolites. Only small, suitably shaped gas molecules can diffuse into the adsorbent whereas other gas molecules are excluded. The second mechanism is based on diffusion kinetics and relies on differences in diffusion rates of molecules into the sorbent. The third mechanism operates through equilibrium, or competitive, adsorption of gases in the mixture and is referred to as equilibrium separation.

Untreated clay minerals have not apparently been studied for the preferential adsorption of gases. However, pillared interlayer clays, or "pillared clays", were studied for these properties. Pillared clays are effective sorbents for kinetic separation of N_2/O_2 in air (Yang and Baksh, 1991), xylene isomers (Yang and Baksh, 1991), as well as CH_4/N_2 and SO_2/CO_2 mixtures (Baksh and Yang, 1992). Recently, the gas adsorption properties of Al-, Cr-, Zr-, and Ti-pillared clays; modified Al-pillared clays, and acid-treated bentonites were reported (Volzone *et al.*, 1997a, 1997b, 1998; Volzone and Ortiga, 1998).

A recent patent application (Thompson *et al.*, 1994) reported the modification of kaolin minerals by aqueous reaction with concentrated KF solution to produce amorphous derivatives "characterized by high specific surfaces and/or high cation exchange capacities". The BET N_2 specific surfaces for the kaolinite and halloysite examples were 100(1) and 167(1) m^2g^{-1}. Transmission electron micrographs of these materials showed a dramatic reduction in particle size upon reaction consistent with the observed specific surfaces being dominated by external surfaces.

The present study explores systematically the gas adsorption properties of these and related amorphous clay mineral derivatives for a range of gases to assess the potential of these derivatives to separate industrial gases.

MATERIALS AND METHODS

Clay mineral starting materials

The four aluminosilicate clay minerals chosen as starting materials were: 1) Skardon-River kaolinite, a poorly crystallized very fine-grained fluvial kaolinite from Skardon River, Far North Queensland, Australia (Wallis, 1997). The clay, known as "Phlofine", was supplied by Australian Kaolin Ltd. and had been processed to <1-μm size fraction, primarily to remove

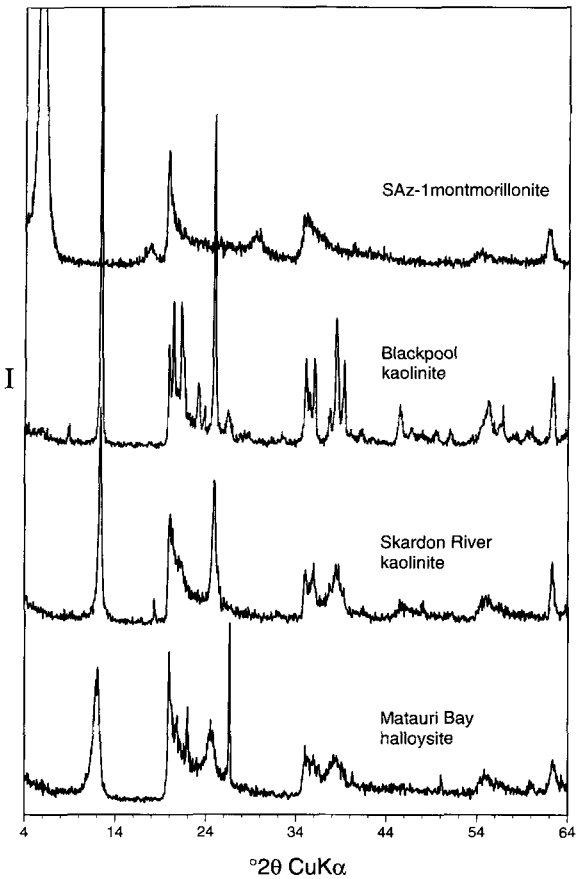

Figure 1. XRD profiles (4–64 °2θ, λ = 1.5418 Å) for the four starting materials.

associated quartz. 2) Blackpool kaolinite, a well-crystallized coarser kaolinite from Blackpool, England. This clay, batch no. RLO 2891, was supplied by E. C. C. International. 3) Matauri-Bay halloysite, a tubular halloysite from Matauri Bay, Northland, New Zealand. The clay, known as "Premium Grade", was supplied by New Zealand China Clays Ltd. and had been processed to remove most of the associated cristobalite and quartz (Harvey *et al.*, 1990). 4) SAz-1 montmorillonite, a Cheto montmorillonite from Apache County, Arizona, USA. The montmorillonite was obtained from the University of Missouri-Columbia, Source Clay Minerals Repository, USA. The powder X-ray diffraction (XRD) profiles for the starting materials are given in Figure 1 and compositions are listed in Table 1.

Synthesis of amorphous derivatives

In each case, the clay mineral and potassium fluoride were thoroughly mixed with water in specific proportions, and the mixture was heated in an open vessel in an oven at 80°C for various times (Table 2). Reaction times were chosen to optimize the yield of amorphous derivatives. The reaction product was then dispersed in 1500 mL of water and allowed to stand for 45 min, during which time the solids settled. The supernatant water was decanted, the solid further rinsed with water, and then separated using a centrifuge. This rinsing step was repeated until no further fluoride could be detected in the elute by the addition of silver nitrate solution, typically after four times.

The resultant solid was dried at 100°C in air. It was a mixture of amorphous derivative and relatively insoluble fluoride by-products. The fluorides were removed by rinsing the solid in 0.02 M potassium hydroxide solution for 30 min at room temperature. A

Table 1. Chemical composition of starting materials and amorphous derivatives.[1]

Sample	wt. %[2]										Atomic ratio	
	Na_2O	MgO	Al_2O_3	SiO_2	K_2O	CaO	TiO_2	Fe_2O_3	F[3]	H_2O[4]	K:Al	Al:Si
$Al_2Si_2O_5(OH)_4$[5]	—	—	45.90	54.10	—	—	—	—	—	13.96	—	1.00
Skardon-River kaolinite	1.32(4)	0.0[6]	44.9(1)	51.1(2)	0.12(3)	0.0[6]	1.58(4)	0.96(9)	—	16.88	0.00	1.04
Blackpool kaolinite	0.6[6]	0.0[6]	44.5(2)	54.2(2)	0.6(1)	0.0[6]	0.21(6)	0.5(1)	—	14.04	0.01	0.97
Matauri-Bay halloysite	0.0[6]	0.0[6]	41.5(3)	58.1(4)	0.0[6]	0.0[6]	0.0[6]	0.45(7)	—	15.38	0.00	0.85
SAz-1 montmorillonite	0.0[6]	6.77(6)	19.6(1)	68.2(2)	0.15(6)	3.4(2)	0.30(9)	1.61(3)	—	23.85	0.02	0.34
SKAD100	0.42(3)	0.0[6]	27.6(2)	45.4(2)	24.3(2)	0.0[6]	1.51(4)	0.8(1)	0.8(2)	14.43	0.95	0.70
SKAD80	0.50(8)	0.0[6]	27.4(2)	46.1(2)	23.7(2)	0.0[6]	1.5(2)	0.87(8)	1.3(2)	15.46	0.93	0.72
BKAD	0.38(4)	0.0[6]	27.9(1)	46.2(3)	25.0(2)	0.0[6]	0.15(6)	0.37(6)	1.9(2)	14.91	0.97	0.71
HAD	0.39(6)	0.0[6]	25.3(2)	51.7(6)	22.2(3)	0.0[6]	0.0[6]	0.33(4)	1.5(2)	12.26	0.95	0.58
MAD	0.0[6]	6.10(4)	15.8(4)	61.8(2)	11.0(4)	3.5(2)	0.30(3)	1.6(2)	3.8(2)	14.31	0.77	0.30

[1] Wt. % as oxide determined by quantitative EDS except for H_2O which was determined by weight loss on ignition (1000°C for 16 h in Pt vessel).
[2] Anhydrous basis.
[3] Wt. % of element.
[4] Total water loss—includes adsorbed, interlayer, and structural water.
[5] Ideal kaolinite.
[6] Below detection.
Note: One standard deviation in the least significant figure is given in parentheses.

https://doi.org/10.1346/CCMN.1999.0470511 Published online by Cambridge University Press

final rinsing of the product with cold water followed, until the pH of the elute dropped to between 10–11. The solid was again separated by centrifuge then dried at 100°C.

Characterization

XRD data were collected at room temperature on a Siemens D5000 diffractometer (Bragg-Brentano) with CuKα radiation (λ = 1.5418 Å). Specimens were prepared using a lightly front-packed mount. Compositions of the samples were determined using a JEOL 6400 scanning electron microscope (SEM) equipped with a Link ATW detector. Quantitative energy dispersive X-ray spectroscopic (EDS) analyses were made at 15 kV and 1 nA with data processed using the Link ISIS system. ZAF corrections were made using the SEM-QUANT software package. Uniaxially pressed pellets of the materials were used for analysis. Low-resolution electron micrographs of the starting materials and their amorphous derivatives were recorded in a JEOL 100 CX transmission electron microscope (TEM). Specimens were dispersed in water and allowed to settle on copper grids supporting holey carbon film. Images were recorded using low illumination to minimize electron-beam damage.

The density of the powder samples was measured by mercury immersion using a Macropore Unit 120 Carlo Erba instrument. Specimens were pretreated at 100°C. The specimen cell was filled with mercury at a pressure of 1 kPa and then vented to atmospheric pressure. Density was obtained by dividing the weight of the sample by the difference between the volume of mercury filling the empty cell and the volume with the sample present.

Equilibrium adsorption was measured using standard volumetric apparatus. Samples were outgassed at 100°C for 12 h prior to measurement. Adsorption was measured at 25°C and 1 kg cm^{-2}. The gases tested for adsorption behavior were N_2, O_2, CH_4, CO, CO_2, and C_2H_2. Adsorption-desorption isotherms were obtained at 77 K with N_2 gas, using a Micromeritics Accusorb instrument. Specific surfaces (BET) were calculated from the first part of the isotherm ($P/P_0 < 0.3$), where P_0 is the vapor pressure of the liquid adsorbate at the temperature of the isotherm. For the kaolin clays and their derivatives, the internal and external surface areas were derived according to the method of Delon *et al.* (1986), which assumes slit shaped pores. The internal and external surface values corresponding to montmorillonite clay were obtained according to the method of Gregg and Sing (1991) whereas it was necessary to use the method of Delon *et al.* (1986) for the montmorillonite derivative.

Differential thermal analysis (DTA), differential thermal gravimetry (DTG), and thermal gravimetric analysis (TGA) data were recorded for each specimen using a Thermal Analyse Netzsch STA 409 instrument.

RESULTS AND DISCUSSION

Amorphous derivatives

Figure 2 presents the XRD profiles for the amorphous derivatives studied for gas adsorption properties. Each derivative from the kaolin-group starting materials shows a predominantly single phase product with a characteristic XRD profile. Minor quartz and cristobalite impurities are present in the halloysite derivative. The montmorillonite derivative shows a mixture of montmorillonite starting material, albeit with a reduction in the *d*(001) from 15.1 to 11.4 Å, represented by the strong non-basal reflections at ~20 °2θ, and amorphous derivative. A higher proportion of montmorillonite amorphous derivative could not be achieved because heating at higher temperature and/or for a longer time produced high proportions of poorly soluble crystalline reaction by-products.

Each kaolin-group derivative shows a single very broad diffraction peak at ~3.1 Å corresponding to the

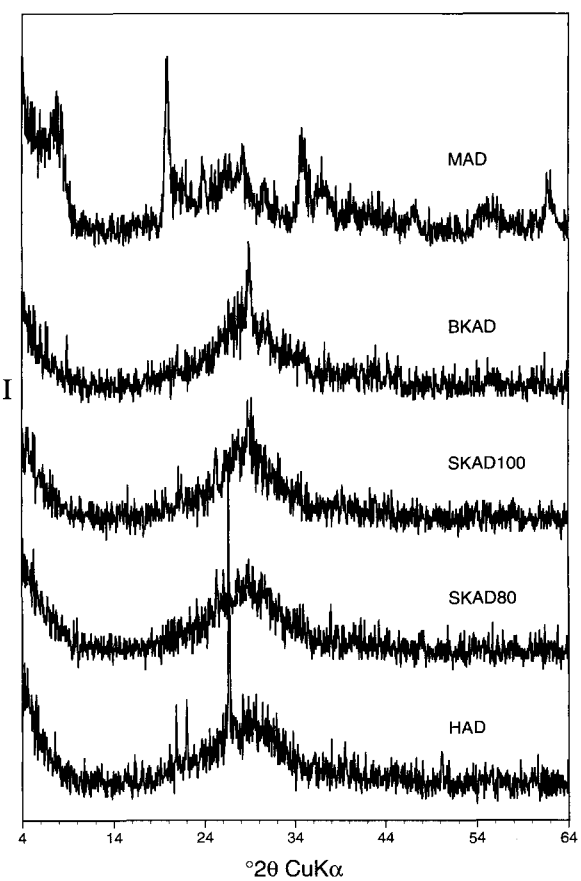

Figure 2. XRD profiles (4–64 °2θ, λ = 1.5418 Å) for the five amorphous derivatives studied for their gas adsorption properties.

https://doi.org/10.1346/CCMN.1999.0470511 Published online by Cambridge University Press

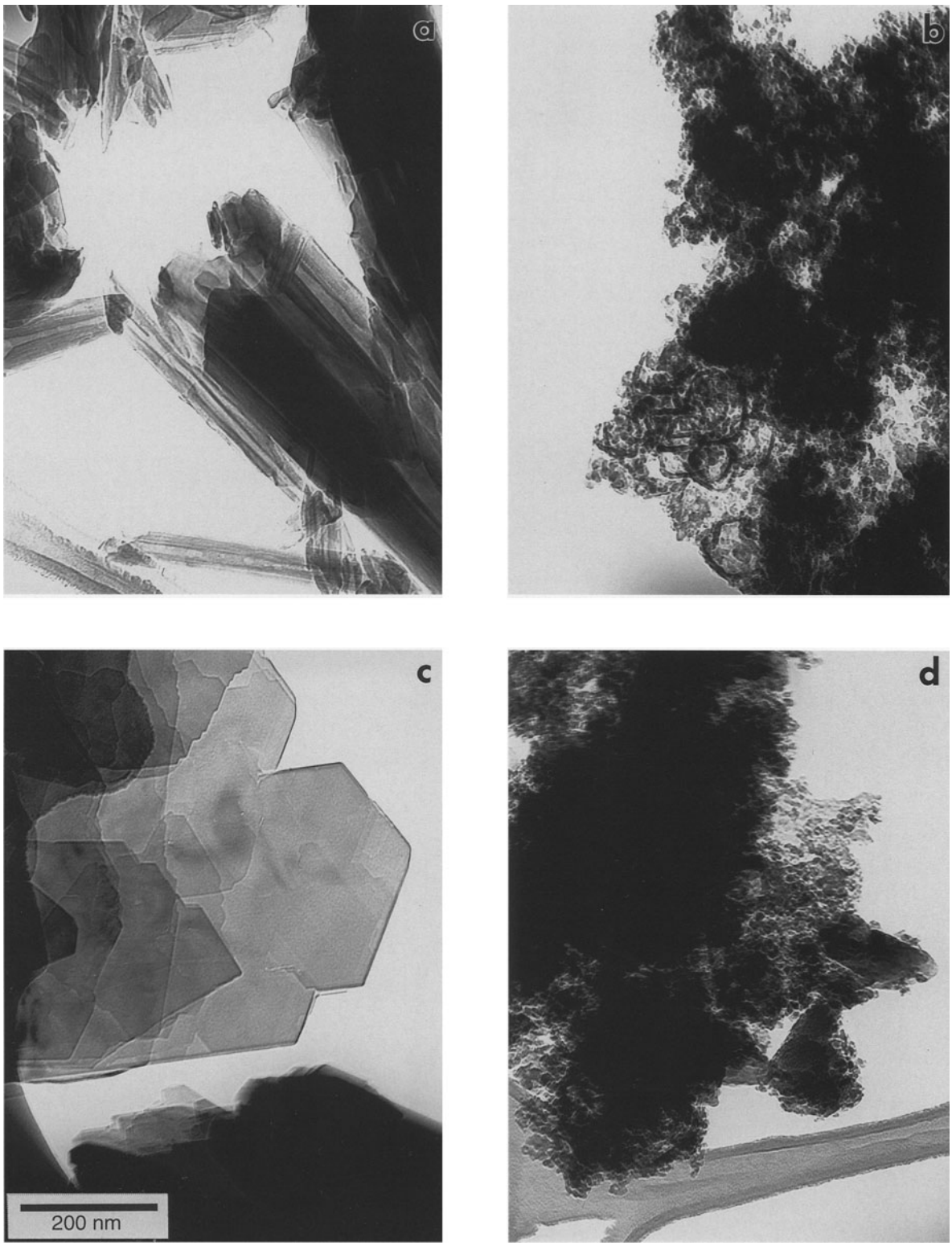

Figure 3. Low-resolution TEM bright field images of the four starting materials (a) Matauri-Bay halloysite, (c) Blackpool kaolinite, (e) Skardon-River kaolinite, and (g) SAz-1 montmorillonite, juxtaposed to typical regions of their corresponding amorphous derivatives (b) HAD, (d) BKAD, (f) SKAD100, and (h) MAD. All images are at the same magnification.

https://doi.org/10.1346/CCMN.1999.0470511 Published online by Cambridge University Press

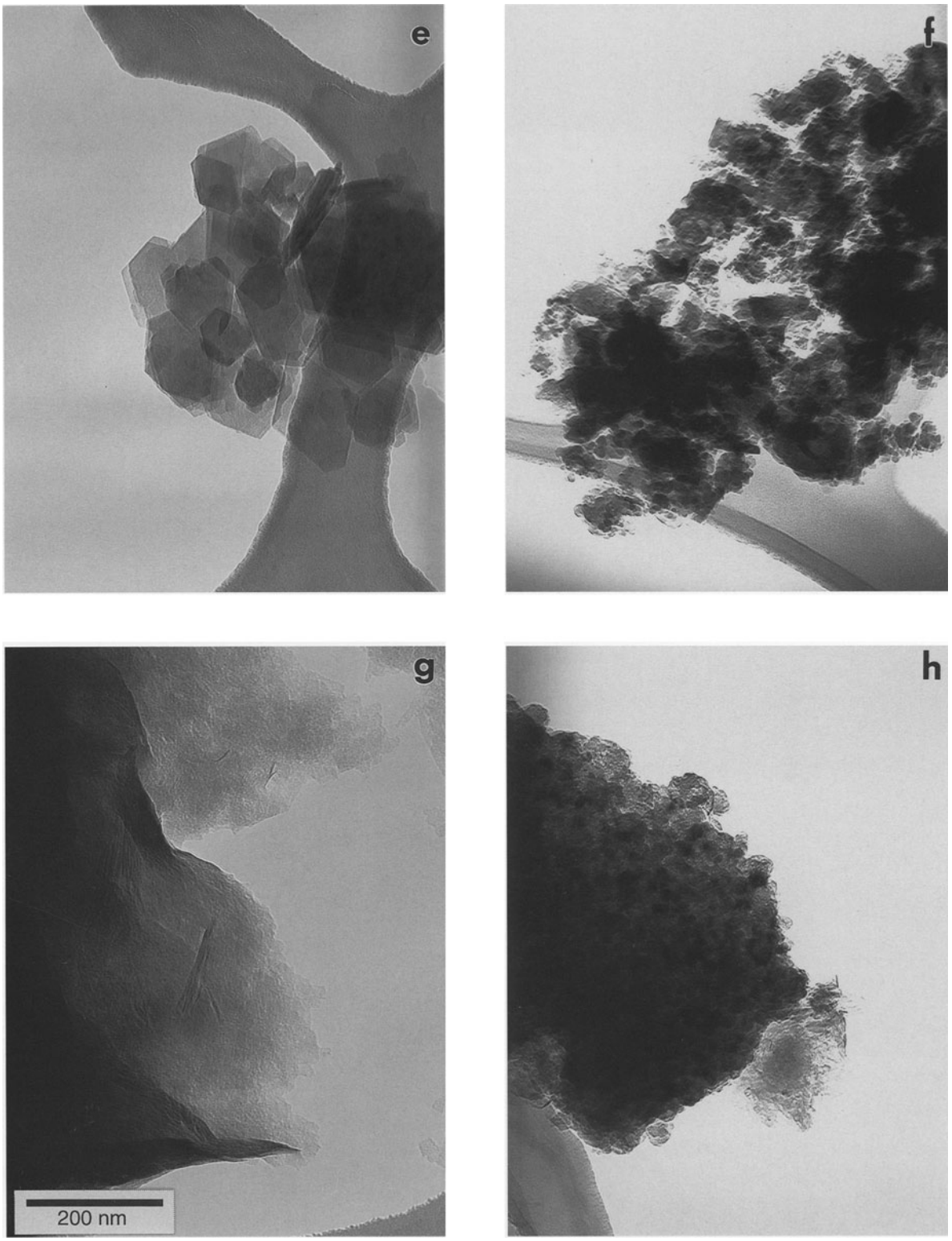

Figure 3. Continued.

https://doi.org/10.1346/CCMN.1999.0470511 Published online by Cambridge University Press

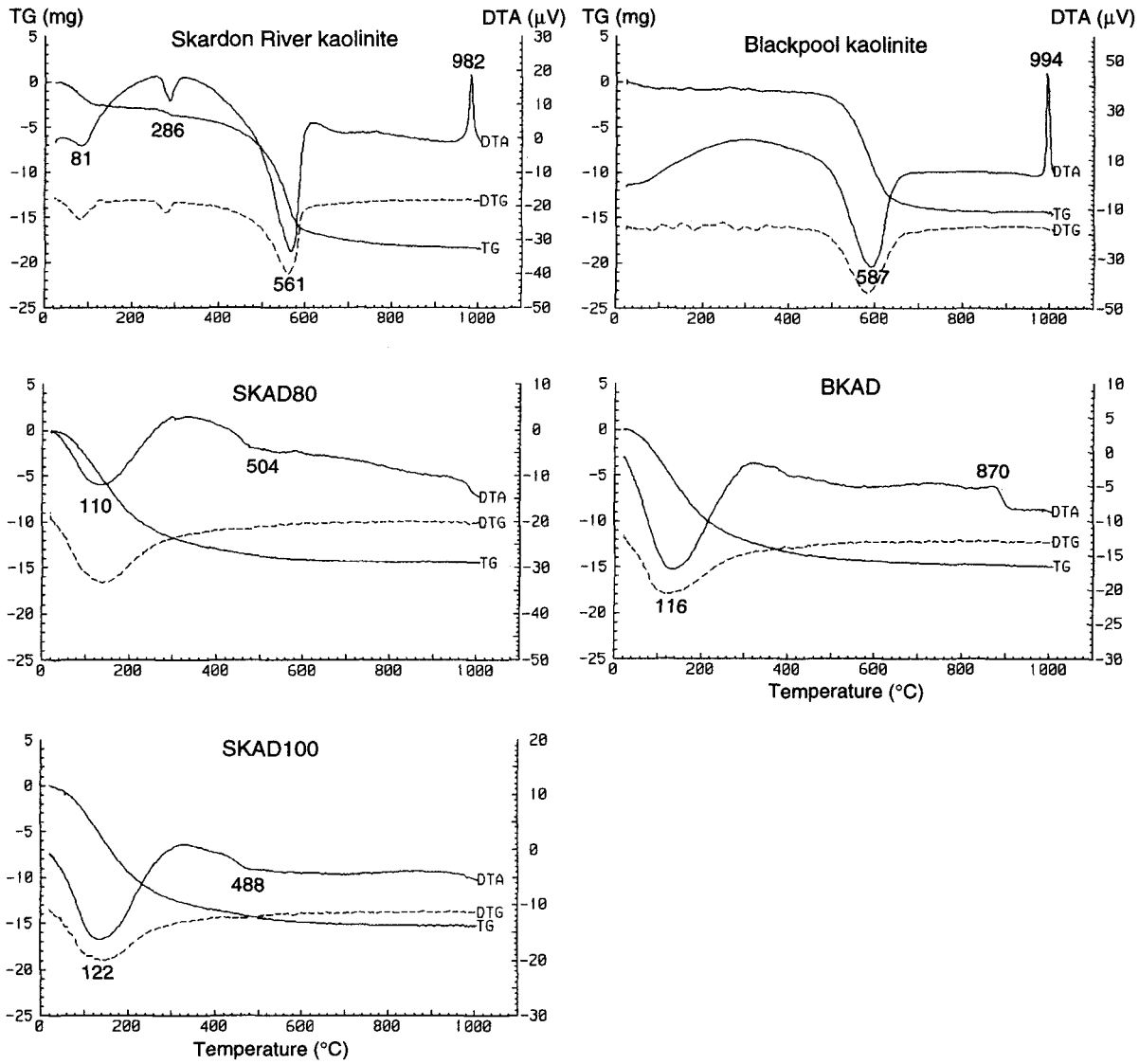

Figure 4. TGA, DTG, and DTA curves for the materials studied. Data for the amorphous derivatives are juxtaposed to their respective starting materials. The temperatures (°C) of the observed endotherms and exotherms for the DTA curves are shown.

102 reflection (d = 3.12 Å) in kalsilite, $KAlSiO_4$ (Perrotta and Smith, 1965), and is similar to the imperfectly crystallized kalsilite prepared by solid-state reaction between intimately mixed kaolinite and K_2CO_3 at 500°C (Thompson *et al.*, 1997). The single broad peak indicates a nascent periodic structure presumably associated with the layers of interstitial and framework cations.

Chemical analysis of the amorphous derivatives

Interpretation of the chemical compositions of the halloysite and montmorillonite amorphous derivatives is complicated by the presence of silica-mineral impurities and unreacted clay, respectively. However, it is clear from the data for the two kaolinite derivatives that there is ~30% reduction in the Al:Si atomic ratio upon reaction to form the derivative. Allowing for the presence of ~8–10 wt. % silica-mineral impurities in the halloysite, a similar reduction in Al:Si ratio would also be observed for the halloysite derivative. The ~30 wt. % Al_2O_3 leached from the clay is observed in the initial unrinsed reaction product as a mixture of relatively insoluble potassium aluminum fluorides, which are subsequently removed by rinsing with alkali.

The K:Al atomic ratio for all four kaolin derivatives ranges between 0.93–0.98. This is consistent with each potassium ion in the derivative being associated with an aluminum in the framework, as is the case in the stuffed silica polymorph kalsilite, $KAlSiO_4$. The ratio is also in agreement with the interpretation of the XRD

https://doi.org/10.1346/CCMN.1999.0470511 Published online by Cambridge University Press

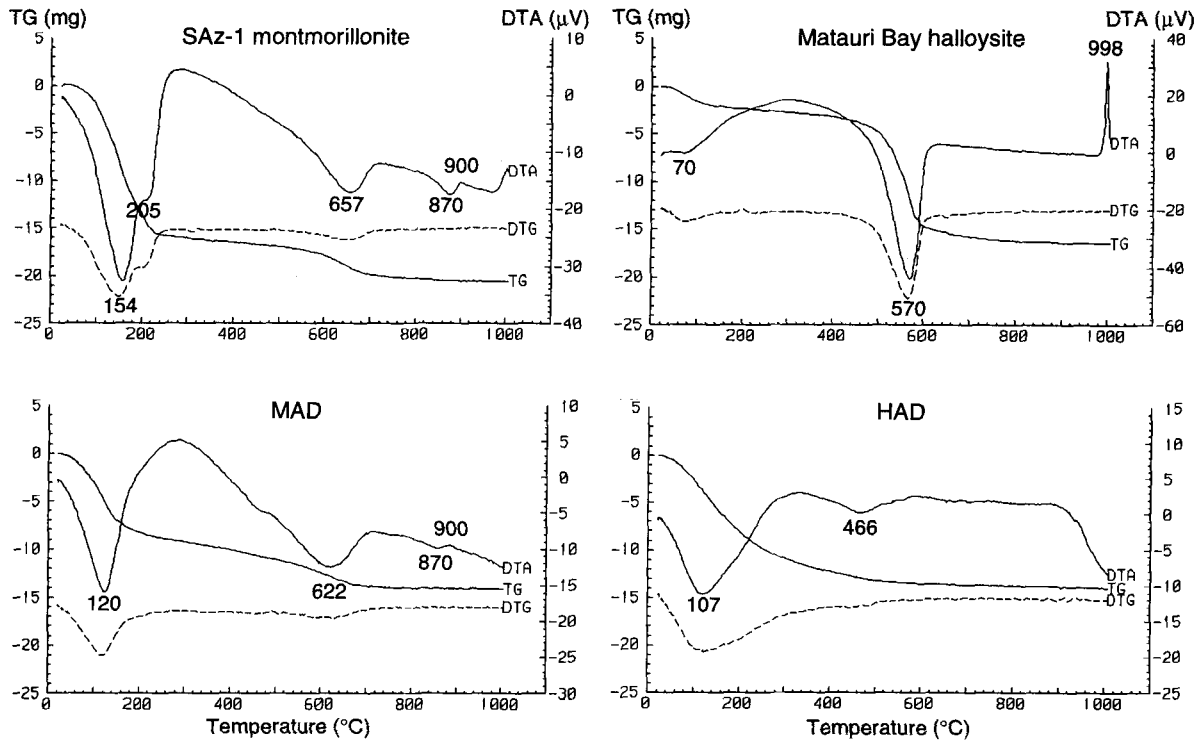

Figure 4. Continued.

data and the previously reported solid state ^{27}Al nuclear magnetic resonance (NMR) data (Thompson *et al.*, 1994), which showed the Al to be tetrahedrally coordinated.

For the montmorillonite derivative, both the change in Al:Si ratio and the resultant K:Al ratio, when compared with the kaolin mineral results, imply incomplete reaction, as observed by XRD.

TEM

Figure 3 shows low resolution TEM bright-field images of the four starting materials juxtaposed to typical regions of their corresponding amorphous derivatives (SKAD80 is not shown but appeared similar to SKAD100). In each case, the characteristic morphology of the respective clays is replaced by agglomerates of very small amorphous particles. The very small dimension of these individual particles is commensurate with the observed large specific surfaces for these derivatives. The large specific surfaces are principally due to external surface.

Each TEM image of the amorphous derivatives of Matauri-Bay halloysite (Figure 3b), Blackpool kaolinite (Figure 3d), and Skardon-River kaolinite (Figure 3f) shows similar degradation of the starting morphology to agglomerates of irregularly shaped particles of 5–20 nm. The tubular morphology of the Matauri-Bay halloysite (Figure 3a) has completely disappeared in the image of its amorphous derivative HAD (Figure 3b). Occasionally remnant ring-like features 50–100 nm in diameter were seen in the HAD specimen. The amorphous derivative of the Blackpool kaolinite (BKAD) (Figure 3d) shows smaller particles than that of the Skardon-River kaolinite (SKAD100) (Figure 3f), though both specimens showed agglomerates commensurate with the size of the kaolinite crystals from which they were formed. Figure 3g shows the typical irregular flakey morphology for

Table 2. Proportions of reagents and reaction conditions.

Starting material	Product label	Reaction mixture (g)			Reaction		Yield (g)
		Clay	KF	H_2O	Temp (°C)	Time (h)	
Skardon-River kaolinite	SKAD100	10	42.0	20	100	2.25	6.70
Skardon-River kaolinite	SKAD80	11	45.0	32	82	32	9.50
Blackpool kaolinite	BKAD	10	42.6	20	110	5.5	8.74
Matauri-Bay halloysite	HAD	10	44.5	20	95	1	7.95
SAz-1 montmorillonite	MAD	10	50.0	20	103	22	8.31

https://doi.org/10.1346/CCMN.1999.0470511 Published online by Cambridge University Press

Table 3. Specimen densities.

Specimen	Density (gcm^{-3})
Skardon-River kaolinite	1.28
Blackpool kaolinite	1.20
Matauri-Bay halloysite	1.32
SAz-1 montmorillonite	1.12
SKAD80	0.52
SKAD100	0.50
BKAD	0.45
HAD	0.39
MAD	1.12

montmorillonite. The MAD specimen showed a significant proportion of unreacted material, but Figure 3h is representative of material which reacted completely. The montmorillonite amorphous derivative did not generally show the same discrete particles observable in the kaolin-group mineral derivatives.

Mercury immersion densities

With the exception of montmorillonite, the densities of the amorphous derivatives were 2.5–3.0 times less than those of the starting materials (Table 3). This behavior indicated important changes in textural characteristics and is consistent with the TEM observations. A higher porosity developed after treatment.

Thermal analyses

Figure 4 presents the combined DTA, DTG, and TGA data for each starting material juxtaposed to their amorphous derivatives. Each kaolin-group mineral shows principal weight loss at 450–600°C associated with the dehydroxylation of the 1:1 layer. This corresponds to the broad endotherm in the DTA curve in each case associated with the kaolinite-metakaolinite and halloysite-metahalloysite phase transitions. The sharp exotherms for each clay at 980–1000°C is associated with the transformation to mullite. The small endotherm at 286°C in the Skardon-River kaolinite corresponds to the decomposition of the Na polyacrylate dispersant remnant in this specimen.

In the TGA curves of the four corresponding amorphous derivatives (HAD, BKAD, SKAD100, and SKAD80), structural-water loss begins almost immediately and is complete by ~500°C. The broad endotherm at 110–120°C in the DTA curves corresponds to this water loss. The very broad exotherm at ~350°C in each case is presumably associated with chemical and structural inhomogeneity of the anhydrous amorphous derivative.

The general similarity between the TGA and DTA data for the montmorillonite and its derivative confirms the XRD, chemical, and TEM observations described above, that the MAD specimen contained a substantial proportion of clay which had not reacted to produce amorphous derivative. Nevertheless the dehydration properties of the unreacted clay have clearly been modified following treatment by the potassium fluoride solution. The predominant water-loss peak for montmorillonite which occurs just above 100°C is related to the evolution of interlayer water. Structural-water is lost at ~600°C. The DTA and TGA curves for the MAD specimen are interpretted as approximate convolutions of the curves for the starting material and an amorphous derivative with thermal characteristics similar to the kaolin amorphous derivatives.

Surface and volume measurements

The various surface and total-volume measurements derived from the adsorption-desorption isotherms are listed in Table 4. For the kaolin-group clays, the total surface areas increased significantly: ~2.5 times in SKAD80 and SKAD100, ~10 times for BKAD, and 3.5 times for HAD. For the montmorillonite derivative, MAD, which contained substantial unreacted clay, the total surface almost halved upon reaction. The increase in surface area for the kaolin-group clays resulted mainly from an increase in external surface. This is consistent with the TEM observations for these specimens. The decrease in surface area for the MAD specimen is due to the loss of internal surface as the external surface actually increases approximately threefold. As for the thermal analysis results, we attribute the decrease to the 'unreacted' clay having been modified following treatment by the potassium fluoride solution.

The total volume increased after reaction for all starting materials with a tenfold increase for the Black-

Table 4. Surface and volume measurements.

Specimen	BET surface (m^2g^{-1})	Total surface (m^2g^{-1})	External surface (m^2g^{-1})	Internal surface (m^2g^{-1})	Total volume (cm^3g^{-1})
Skardon-River kaolinite	25	22.5	12.6	9.9	141
Blackpool kaolinite	11	10.1	6	4.1	34
Matauri-Bay halloysite	26	24.3	20	4.3	68
SAz-1 montmorillonite	81	78	7	71	92
SKAD80	66	59	47	12	209
SKAD100	63	57.1	37.5	19.6	202
BKAD	108	106.4	89.2	17.2	340
HAD	89	89	72.4	16.6	460
MAD	38	38	21	17	246

Table 5. Equilibrium gas-adsorption measurements (mmol g^{-1}).

Specimen	N_2	O_2	CH_4	CO	CO_2	C_2H_2	CO_2/CH_4	C_2H_2/CH_4
Skardon-River kaolinite	0.019	0.024	0.024	0.069	0.056	0.067	2.33	2.79
Blackpool kaolinite	0.024	0.017	0.017	0.027	0.035	0.056	2.06	3.29
Matauri-Bay halloysite	0.026	0.021	0.019	0.064	0.040	0.051	2.11	2.68
SAz-1 montmorillonite	0.031	0.028	0.020	0.033	0.210	0.180	10.50	9.00
SKAD80	0.050	0.052	0.058	0.058	0.226	0.180	3.90	3.10
SKAD100	0.050	0.053	0.053	0.058	0.272	0.185	5.13	3.49
BKAD	0.064	0.064	0.064	0.069	0.297	0.256	4.64	4.00
HAD	0.074	0.079	0.074	0.089	0.294	0.259	3.97	3.50
MAD	0.026	0.031	0.026	0.042	0.201	0.164	7.73	6.31

pool kaolinite derivative, sevenfold for the halloysite derivative, ~50% increase for the two Skardon-River kaolinite derivatives, and ~150% increase for the montmorillonite. For the kaolin-group mineral derivatives, there is an inverse and consistent relationship between the observed densities (Table 3) and the total volume measurements. Note that the volume results were obtained using N_2 gas temperature at ~77 K and the density was obtained with Hg at room temperature (~298 K).

Equilibrium adsorption measurements for N_2, O_2, CH_4, CO, CO_2, and C_2H_2

Equilibrium adsorption data are summarized in Table 5. For all starting materials, except for the montmorillonite, the level of adsorption for all gases is relatively low. For the montmorillonite, the CO_2 and C_2H_2 adsorption is 4–6 and 2.5–3.5 times, respectively, the levels of the kaolin-group clays.

The relative increases in adsorption for each gas are summarized in Table 6. The amorphous derivatives of the kaolin-group minerals show increases in CO_2 and C_2H_2 adsorption of 4.0–8.5 times and 2.7–5.1 times, respectively. The montmorillonite derivative shows no increase in adsorption over the starting material. Of the kaolin-group mineral derivatives, the HAD and BKAD show the most striking increases in gas adsorption values relative to the starting material.

Correlation of gas adsorption with sample surface and volume

In Figure 5a the total surface *vs.* gas retention in mmol g^{-1} is plotted. This plot shows approximately linear correlation between the surfaces of the nine materials and the level of gas adsorbed for each of the six gases. The correlation was best for the BET or the total surface, rather than the external or internal surface areas (not shown), which implies that the gas adsorption behavior of internal and external surfaces is similar. The data for CO_2 and C_2H_2 clearly show the greatest slope relative to the other gases.

Table 6. Gas-adsorption ratio (product/starting material).

Specimen	N_2	O_2	CH_4	CO	CO_2	C_2H_2
SKAD80	2.6	2.1	2.4	0.8	4.0	2.7
SKAD100	2.6	2.2	2.2	0.8	4.8	2.8
BKAD	2.7	3.8	3.8	2.6	8.5	4.6
HAD	2.9	3.8	3.9	1.4	7.3	5.1
MAD	0.8	1.1	1.3	1.3	1.0	1.2

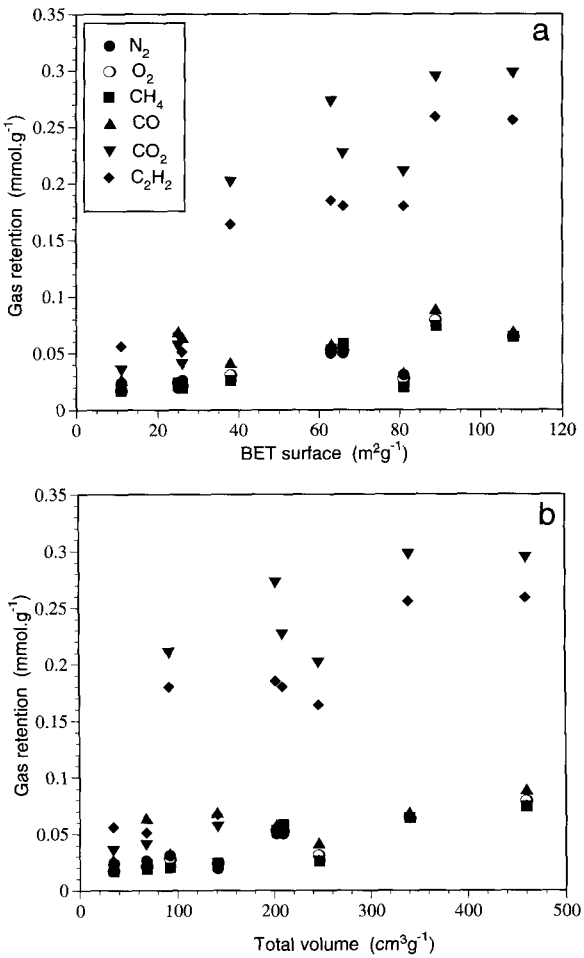

Figure 5. Correlation plots of (a) the total surface in m^2g^{-1} *vs.* gas retention in mmol g^{-1} and (b) the total volume cm^3g^{-1} *vs.* gas retention in mmol g^{-1} using the data listed in Tables 4 and 5.

https://doi.org/10.1346/CCMN.1999.0470511 Published online by Cambridge University Press

Figure 5b plots the total volume *vs.* gas retention and shows a similar approximately linear correlation to Figure 5a, the main difference being that the increase in total volume is larger than the increase in surface area (Table 4). This may indicate that in the clay derivatives the mesopore or macropore volume is significant. Note that the total volume includes the volume of micropores, mesopores, and macropores but does not identify the individual contribution of each. The high CO_2 and C_2H_2 gas adsorption values for montmorillonite and its derivative are observed in Figure 5a and 5b. There is apparently no correlation between surface area or total volume and ratios of gas loading (see Table 5) for CO_2/CH_4 and C_2H_2/CH_4.

Levels of gas retention and selectivity compared with other adsorbents

Previous studies (*e.g.,* Baksh and Yang, 1992) showed that the level of gas adsorption varies according to the size of the gas molecule and the physicochemical characteristics of the adsorbent (clays, modified clays, carbon, zeolites, *etc.*). Owing to the amorphous nature of the clay mineral derivatives, we have only limited data on the structure and chemistry of the surfaces and pore-size distribution. Nevertheless, it is useful to compare the gas adsorption behavior of these materials with pillared clays whose structure, chemistry, surface areas, and pore-size distributions are known.

The gas retention values of the kaolinite derivatives were similar to those found by Baksh and Yang (1992) and Volzone *et al.* (1997a, 1997b, 1998) for various pillared clays. Baksh and Yang (1992) reported gas adsorption levels for N_2, O_2, CH_4, and CO_2 at P = 1 atm. and 298 K for Zr-, Al-, Cr-, Fe-, and Ti-pillared clays. The levels of adsorption for these four gases by the present four kaolin-group derivatives most closely matched the levels reported for Ti- and Fe-pillared clays, which is surprising given that the BET surface areas of the pillared clays (Baksh and Yang, 1992) were typically 2–4 times larger than those reported here. Volzone *et al.* (1997a, 1997b, 1998) also reported similar levels of adsorption for Al-, Cr-, Zr-, and Ti-pillared clays under the same experimental conditions used in the present study with the highest levels of CO_2 and C_2H_2 adsorption, 0.33 and 0.35 mmol g^{-1}, respectively, for a modified Al-pillared clay.

The CO_2/CH_4 gas adsorption ratios reported by Baksh and Yang (1992) for Ti-pillared clay and Fe-pillared clay were ~2.95 and 2.0, respectively. For the various pillared clays studied by Volzone *et al.* (1997a, 1997b, 1998) the CO_2/CH_4 ratio ranged between 2.3–4.5 with a high value of 6.6 for modified Al-pillared clay. These data compare with a range of 3.9–5.1 for the kaolin-group derivatives. The montmorillonite and its derivative showed higher CO_2/CH_4 gas adsorption ratios (Table 5) but at lower loadings than the kaolin-group derivatives.

Adsorbents were investigated for use in the separation of gas mixtures. Molecular-sieve carbon has been used for kinetic separation of air (Patel *et al.,* 1972) and CO_2/CH_4 mixtures (Kapoor and Yang, 1989). The latter authors observed similar gas adsorption ratios to those reported here for amorphous clay derivatives. In principle, the gas loadings and adsorption ratios observed for the materials studied here should make them suitable for CO_2/CH_4 separation. However, unlike Al-pillared clays (Baksh and Yang, 1992) amorphous kaolin-group derivatives showed no CH_4/N_2 selectivity.

CONCLUSIONS

The clay derivative materials studied here have apparent potential for selective gas adsorption for certain gas mixtures. For situations where separation of N_2, O_2, CO, or CH_4 from CO_2 or C_2H_2 is required, then these amorphous clay derivatives may be suitable. A gas adsorption ratio of 3 is considered to be the threshold for commercial viability (Baksh and Yang, 1992).

For the nine materials studied, the levels of adsorption for the various gases correlated approximately linearly with the BET surface areas. If the surface areas of the amorphous clay derivatives can equal or surpass those reported in the original patent (Thompson *et al.,* 1994) then they are likely to compete favorably with other comparable adsorbents such as molecular-sieve carbon and pillared clays. Higher surface areas for kaolin-group amorphous derivatives can be obtained by allowing the kinetically-controlled reaction to proceed further at the expense of producing a higher proportion of poorly soluble reaction by-products.

Further variations of synthesis conditions and starting materials, surface measurement, pore-size characterization, and gas adsorption work is required to understand the mechanism of selective gas adsorption and to explore the maximum levels of gas retention attainable for this class of modified clay minerals.

ACKNOWLEDGMENT

The assistance of S. Conconi with the recording of thermal analysis data is appreciated.

REFERENCES

Baksh, M.S.A. and Yang, R.T. (1992) Unique adsorption properties and potential energy profiles of microporous pillared clays. *American Institute of Chemical Engineers Journal,* **38,** 1357–1368.

Delon, J.F., Lietard, O., Cases, J.M., and Yvon, J. (1986) Determination of porosity of platy materials using slit-shaped and bevelled pores. *Clay Minerals,* **21,** 361–375.

Gregg, S.L. and Sing, K.S.W. (1991) *Adsorption Surface Area and Porosity, 2nd edition.* Academic Press, London, 303 pp.

Harvey, C.C., Townsend, M.G., and Evans, R.B. (1990) The halloysite clays of Northland, New Zealand. *The Austra-*

lasian Institute of Mining and Metallurgy Annual Conference, Rotorua, New Zealand, 229–238.

Kapoor, A. and Yang, R.T. (1989) Kinetic separation of methane-carbon dioxide mixture by adsorption on molecular sieve carbon. *Chemical Engineering Science,* **44,** 1723–1733.

Patel, R.L., Nandi, S.P., and Walker, P.L., Jr. (1972) Molecular sieve characteristics of slightly activated anthracite. *Fuel,* **51,** 47–51.

Perrotta, A.J. and Smith, J.V. (1965) The crystal structure of kalsilite, $KAlSiO_4$. *Mineralogical Magazine,* **35,** 588–595.

Thompson, J.G., Mackinnon, I.D.R., Koun, A., and Gabbitas, N. (1994) Kaolin derivatives. PCT patent application, WO 95/00441 AU94/00323.

Thompson, J.G., Melnitchenko, A., Palethorpe, S.R., and Withers, R.L. (1997) Zeolitic behaviour in stuffed silica polymorphs. *Journal of Materials Chemistry,* **7,** 673–679.

Volzone, C. and Ortiga, J. (1998) Adsorciones de gases en bentonitas modificadas. *9 Congreso Internacional de Cerámica y 3 del Mercosur,* Olavarría, Argentina, 27–29 May 1998, 19–23.

Volzone, C., Ortiga, J., Garrido, L.B., Hipedinger, N.E., and Pereira, E. (1997a) Síntesis de arcillas pilareadas con Al, Cr y Zr para su utilización como adsorbentes. *Programa Iberoamericano de Ciencia y Tecnología para el Desarrollo (CYTED),* Subprograma V. Catálisis y Adsorbentes, Proyecto V.3., Meeting: Colombia, Bogotá, 9–11 abril 1997, 1–7.

Volzone, C., Ortiga, J., Garrido, L.B., Hipedinger, N.E., and Meroni, A.L. (1997b) Síntesis de arcillas pilareadas con Al, Zr y Ti para su utilización como adsorbentes. *Programa Iberoamericano de Ciencia y Tecnología para el Desarrollo (CYTED),* Subprograma V. Catálisis y Adsorbentes, Proyecto V.3., Meeting: La Habana, Cuba, 14–17 de setiembre 1997, 1–7.

Volzone, C., Ortiga, J., and Garrido, L.B. (1998) Síntesis de arcillas pilareadas con Al y modificadas para su utilización como adsorbentes. *Programa Iberoamericano de Ciencia y Tecnología para el Desarrollo (CYTED),* Subprograma V. Catálisis y Adsorbentes. Proyecto V.3., Meeting: Carabalieda, Venezuela, 24–27 febrero 1998, 1–5.

Wallis, D.S. (1997) Queensland minerals for the 21st century. *Publications of the Australasian Institute of Mining and Metallurgy,* **1/97,** 33–42.

Yang, R.T. (1987) *Gas Separation by Adsorption Processes.* Butterworth, Boston, 368 pp.

Yang, R.T. and Baksh, M.S.A. (1991) Pillared clays as a new class of sorbents for gas separation. *American Institute of Chemical Engineers Journal,* **37,** 679–686.

(Received 11 June 1998; accepted 14 April 1999; Ms. 98-074)